Scripta Materialia 152 (2018) 94–97

Contents lists available at ScienceDirect

Scripta Materialia

journal homepage: www.elsevier.com/locate/scriptamat

Regular article

Dependence of stacking faults in gamma matrix on low-cycle fatigue behavior of a Ni-based single-crystal superalloy at elevated temperature

X.G. Wang [a,*], J.L. Liu [a], J.D. Liu [a], Y.Z. Zhou [a,*], J.G. Li [a,*], X.F. Sun [a], J.H. Do [b], B.G. Choi [b], I.S. Kim [b], C.Y. Jo [b]

[a] Institute of Metal Research, Chinese Academy of Sciences, 72 Wenhua Road, Shenyang 110016, China
[b] High Temperature Materials Research Group, Korea Institute of Materials Science, 797 Changwon daero, Changwon 641-831, Gyeongnam, Republic of Korea

ARTICLE INFO

Article history:
Received 6 March 2018
Accepted 13 April 2018
Available online xxxx

Keywords:
Single-crystal superalloy
LCF behavior
Deformation mechanism
Stacking faults

ABSTRACT

The LCF behavior of a fourth-generation Ni-based single-crystal superalloy at elevated temperature with different total strain amplitudes has been studied. Notably, the experimental alloy demonstrated a significant work hardening behavior with the total strain amplitude increasing. A great number of SFs with different configurations in the γ matrix was observed. The nature of work hardening was conclusively shown to be dependent upon the high density of SFs and Lomer-Cottrell dislocations in the γ matrix, which is rarely reported previously. This finding reported in this work provides us a new idea on high performance single-crystal superalloy design.

Nickel-based single crystal (SX) superalloys are important structure materials for applications in the hot zone of aircraft gas turbine engines, e.g. blades and vanes, since they have highly desirable material properties at elevated temperatures, such as excellent resistance to creep, thermal/mechanical fatigue and corrosion [1–3]. These excellent properties of SX superalloys derive from the chemical compositions and the unique gamma/gamma-prime two-phase microstructure [1–5]. In order to obtain the optimal comprehensive mechanical properties, the size, distribution and volume fraction of γ′ precipitates and the width of γ matrix should be elaborately tailored by reasonable ratio of elements and heat-treatment process [6–8]. The macroscopic deformation response and microscopic deformation mechanisms are mainly controlled by the factors abovementioned.

During in-service, the high temperature components of gas turbine engines are subjected to a series of complex operating conditions, including corrosion, oxidation, cyclic loading and plastic deformation at elevated temperatures [3,9,10], etc. Among them, the cyclic stresses (alternating stress), result from startup, accelerate, decelerate and shutdown procedures, play a vital role on the reliability of hot components. Thus, the related low-cycle fatigue (LCF) has been an area of ever-growing interest for the past several decades [11–28]. As a matter of fact, the fundamental mechanical fatigue mechanisms have been established through the extensive study on single-crystals, bicrystals, and polycrystals of FCC metals (e.g., Cu [19,20], Ni [21], Ag [21], Cu-Al alloy [22] and Al-Cu alloy [23,24] etc.). However, although superalloys are the category of FCC structure, the special two-phase microstructure and high content of refractory elements determine that they have their own deformation characteristics. Compared to other metals or alloys as abovementioned, less LCF tests have been conducted on Ni-base SX superalloys [13,15,18] and many complicated deformation mechanisms are still not clear. On the other hand, with the addition of Ru, the stacking fault energy (SFE) of SX superalloys was further significantly decreased [15,25]. Thus, the deformation mechanism of Ru-containing superalloys might be different from the studies conducted previously and own their characteristics. Study on the superalloys with a low SFE contributed to understanding of the deformation and failure mechanisms of the fourth-generation SX superalloys. In turn, these studies may have a guiding significance for design of the new alloys. It is therefore a matter of interest to study the LCF behavior related to a Ru-containing fourth-generation SX superalloy.

Herein, an experimental SX superalloy with 3 wt% Ru-containing (3Ru alloy) was used to study the LCF deformation mechanisms. The nominal chemical composition of the experimental alloy is given in Table 1. The preparation, full heat treatment processes of this alloy were described elsewhere [25]. The cylindrical specimens used in this work along the [001] direction for LCF tests have a gauge length and diameter of 15 and 6 mm, respectively. Before the LCF tests, mechanical and electrochemical polishing were conducted on all the specimens to prevent premature crack initiation at the surface-machined scratches. Series of LCF tests were conducted for these specimens using a MTS810 servo-hydraulic testing machine under different total strain ($\Delta\varepsilon_t$ = 1.3%, 1.6%, and 2.0%) in air at 900 °C. A triangle waveform with a constant strain rate of 5×10^{-3} s^{-1} and strain ratio of R = −1 was used in this work. After LCF failure, the thin foils for transmission electron microscopy (TEM) were sectioned perpendicular to the stress axis from the deformed samples. The thin foils were mechanically

* Corresponding authors.
E-mail addresses: xgwang11b@imr.ac.cn, (X.G. Wang), yyzhou@imr.ac.cn, (Y.Z. Zhou), jgli@imr.ac.cn. (J.G. Li).

https://doi.org/10.1016/j.scriptamat.2018.04.020
1359-6462/

Table 1
Nominal chemical composition (wt%) of the experimental superalloy investigated.

Alloy	Co	Al	Cr + Mo + W + Ta	Re	Ru	Ni
3Ru	12	6	19.4	5.4	3	Bal.

polished down to a thickness of 50 μm, and then jet polished in a solution of 20% perchloric acid and 80% methanol (v/v) at a temperature of −25 °C and a voltage of 20 V. The microstructural configurations of all samples were examined using a JEM-2100F scanning transmission electron microscope (STEM) operating at 200 kV.

In the most area of the alloy, after complete heat treatment, no dislocation is observed in the γ or γ′ phase, as shown in Fig. 1. However, some extended dislocations (SF coupled partial dislocations) in the γ matrix are occasionally observed (Fig. 1 inset). The formation of stacking faults (SFs) after heat-treated is a very unusual feature, indicating a very low SFE of the γ matrix. It is considered that this deformation mechanism might be of vital importance for plastic deformation. It is precisely because of this character, as expected, the LCF deformation mechanisms of the experimental superalloy is obviously different from other generation single-crystal superalloys. The related microstructure analysis will be conducted in detail in the following sections.

Cyclic stress response curves and plastic strain curves of the experimental superalloy under different tests conditions are present in Fig. 2. By comparing the cyclic stress response curves, it can be found that cyclic harding phenomena become more significant and the fatigue life gradually decreases with the increasing of total strain amplitudes. Clearly, these cyclic stress response curves possess their own characters: (i) the response curve with $\Delta\varepsilon_t = 1.3\%$ is relatively stable in the whole cycle process, although a very weak cyclic harding occurs after LCF approximately 10 cycles; (ii) a certain cyclic harding takes place in the wake of a very short cyclic stability stage (about 2 cycles) in the response curve with $\Delta\varepsilon_t = 1.6\%$; (iii) after a short significant cyclic harding in the initial cycles (<5 cycles), the experimental alloy towards a long cycle stability stage quickly, and cyclic softening appears only at the end of the LCF test ($\Delta\varepsilon_t = 2.0\%$). The cyclic stress response curve characters of this experimental alloy is different from other SX alloys, which shows obvious cyclic softening behavior with the increasing of the total strain amplitude [26–28]. Previous studies considered that the initial softening behavior might be derived from the rapid formation of γ/γ′ interface dislocation networks [26], and the following slow softening behavior can be attributed to the microstructural evolution process of time-dependent rafting of γ′ precipitates [29]. Herein, we hold the point that the initial harding phenomenon of this experimental alloy investigated in this work under current conditions might be correlated with the formation of a large number of extended dislocations. The movement of following dislocations would be prevent by these SFs and partial dislocations. Consequently, the more SFs in the γ matrix, the more significant cyclic harding. Fortunately, this viewpoint is definitely confirmed by the microstructure observation using TEM and it will be discussed in the following sections.

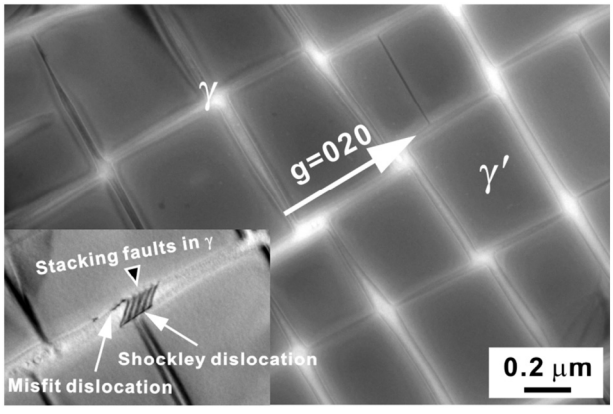

Fig. 1. TEM microstructure of the experimental single-crystal superalloy after heat treatment. Beam ≈ [001].

The mean stress under different total strain amplitude of 1.3%, 1.6% and 2.0% are about 600, 700 and 950 MPa (Fig. 2a), respectively, whereas the yield strength of the experimental alloy at 900 °C is about 890 MPa [30]. Consequently, it can be deduced that during $\Delta\varepsilon_t = 1.3\%$ and 1.6%, the LCF process is dominated by the elastic deformation, and during the $\Delta\varepsilon_t$ increasing to 2.0%, obvious plastic deformation will take place. The plastic strain amplitude ($\Delta\varepsilon_p/2$) agrees well with the deduction abovementioned, as shown in Fig. 2b. Clearly, the larger plastic strain amplitude is, the shorter of the LCF fatigue life is.

Deformation microstructures of the experimental alloy after LCF failure under different total strain amplitudes at 900 °C are shown in Fig. 3. Comparing the deformation microstructures, it can be found that the γ′ phase cutting events by the a⟨011⟩ superdislocations (the APB coupled pairs of a/2⟨011⟩ dislocations) or the a/3⟨112⟩ partial dislocations (leaving SFs in the γ′ phase, as marked by the white triangle with black border) under three different total amplitudes have no significant difference. Herein, it should be noted that the a⟨011⟩ superdislocations are invisible under the operation vector of $\vec{g} = 200$. However, the blurring contrast of the end of truncated dislocation still can be seen, as marked by the red circles in Fig. 3c. In fact, if tilting the specimen these superdislocations show a strong contrast under other operation vectors, e.g. $\vec{g} = 020$ or 220. The only remarkable difference is that the numbers and morphologies of SFs in the γ matrix are totally different from each other. The number of SFs presents in the γ matrix increase significantly with the total strain amplitudes increasing, as marked by black triangles with white border in Fig. 3a–c, suggesting formation of SFs is a very important deformation mechanism for the Ru-containing superalloy studied in this work. After projected on the (001) plane, the SF fringes in the γ matrix are mainly along the [110] and $[\bar{1}10]$ directions, demonstrating at least two slip systems operate. Because of this extending behavior of the SFs, many interesting phenomena are observed in the γ matrix. Clearly, if the TEM foil is very thin, part of the SFs in the γ matrix will be subtracted during twin-jet polishing process. Thus, the thickness which perpendicular to the extending direction on the slip plane of these SFs is extremely thin, and only one or two bright-dark fringes can be observed (seems like a single dislocation), as shown in Fig. 3d marked by a red dashed box.

What interests us more is that in the thinner area these SFs can be divided into two types according to their configurations (Fig. 3d): (i) with the "straight" fringe (marked by "4" and "N" in Fig. 3d); (ii) with the "zigzag" fringe and this type of SFs rarely reported previously (marked by "1", "2", "3" and "M" in Fig. 3d). It is easy to understand the formation mechanism of the SFs with "straight" fringe, and they usually formed in the following way:

$$a/2\langle 011\rangle \rightarrow a/6\langle 112\rangle + SF + a/6\langle 121\rangle \text{in } \gamma \quad (1)$$

However, the formation mechanism of the SFs with "zigzag" fringe is still puzzling and no direct evidence link to this formation process is proven. Despite all that, one possible formation mechanism can be given which schematically illustrated in Fig. 4. Two perfect dislocations with the Burgers vector of $a/2[\bar{1}01]$ and $a/2[0\bar{1}\bar{1}]$ lie on the (111) and $(11\bar{1})$ plane, respectively, and then dissociate as follows (Fig. 4a):

$$a/2\left[\bar{1}01\right] \rightarrow a/6\left[\bar{1}\bar{1}2\right] + SF(I) + a/6\left[\bar{2}11\right] \quad (2)$$

$$a/2\left[0\bar{1}\bar{1}\right] \rightarrow a/6\left[1\bar{2}\bar{1}\right] + SF(II) + a/6\left[\bar{1}\bar{1}2\right] \quad (3)$$